JBC RESEARCH ARTICLE

# Imaging of anthrax intoxication in mice reveals shared and individual functions of surface receptors CMG-2 and TEM-8 in cellular toxin entry

Received for publication, June 17, 2021, and in revised form, November 12, 2021 Published, Papers in Press, December 4, 2021,
https://doi.org/10.1016/j.jbc.2021.101467

**Carly Merritt[1,‡], Elizabeth M. Chun[1,‡], Rasem J. Fattah[2], Lakmali M. Silva[1], Quinn Q. Ma[2], Mahtab Moayeri[2], Dennis Paliga[3], Sebastian Neumann[3], Rolf Heumann[3], Stephen H. Leppla[2], and Thomas H. Bugge[1,*]**

*From the [1]Proteases and Tissue Remodeling Section, National Institute of Dental and Craniofacial Research, and [2]Laboratory of Parasitic Diseases, National Institute of Allergy and Infectious Diseases, National Institutes of Health, Bethesda, Maryland, USA; [3]Department of Biochemistry II – Molecular Neurobiochemistry, Faculty of Chemistry and Biochemistry, Ruhr-Universität Bochum, Bochum, Germany*

Edited by Eric Fearon

***Bacillus anthracis*** **lethal toxin and edema toxin are binary toxins that consist of a common cell-binding moiety, protective antigen (PA), and the enzymatic moieties, lethal factor (LF) and edema factor (EF). PA binds to either of two receptors, capillary morphogenesis protein-2 (CMG-2) or tumor endothelial marker-8 (TEM-8), which triggers the binding and cytoplasmic translocation of LF and EF. However, the distribution of functional TEM-8 and CMG-2 receptors during anthrax toxin intoxication in animals has not been fully elucidated. Herein, we describe an assay to image anthrax toxin intoxication in animals, and we use it to visualize TEM-8- and CMG-2-dependent intoxication in mice. Specifically, we generated a chimeric protein consisting of the N-terminal domain of LF fused to a nuclear localization signal-tagged Cre recombinase (LFn-NLS-Cre). When PA and LFn-NLS-Cre were coadministered to transgenic mice expressing a red fluorescent protein in the absence of Cre and a green fluorescent protein in the presence of Cre, intoxication could be visualized at single-cell resolution by confocal microscopy or flow cytometry. Using this assay, we found that: (a) CMG-2 is critical for intoxication in the liver and heart, (b) TEM-8 is required for intoxication in the kidney and spleen, (c) CMG-2 and TEM-8 are redundant for intoxication of some organs, (d) combined loss of CMG-2 and TEM-8 completely abolishes intoxication, and (e) CMG-2 is the dominant receptor on leukocytes. The novel assay will be useful for basic and clinical/translational studies of** ***Bacillus anthracis*** **infection and for clinical development of reengineered toxin variants for cancer treatment.**

Anthrax is contracted through inhalation, ingestion, or cutaneous inoculation of endospores of the Gram-positive bacterium *Bacillus anthracis*. Spores germinate following their introduction to the body and disseminate to cause a systemic infection, which, if left untreated, is associated with high mortality rates. Upon the death of the host, *Bacillus anthracis* forms spores that are resistant to chemical insults, heat exposure, and dehydration and remain infectious for long periods (1, 2).

The virulence of *Bacillus anthracis* results from the release of three proteins into the circulation: protective antigen (PA), lethal factor (LF), and edema factor (EF). These three proteins are individually nontoxic, and PA combines with either LF to form anthrax lethal toxin or with EF to form anthrax edema toxin. The systemic administration of anthrax toxin to animals closely mimics experimental infection with *Bacillus anthracis*, and vaccination against the toxin components is protective, indicating that anthrax is largely a toxin-mediated disease (1, 2). Anthrax toxins exert their cytotoxic actions in a three-step activation process that involves: (a) the binding of PA to the surface of target cells, (b) the translocation of LF and EF to the cytoplasmic compartment of the target cells, and (c) the enzymatic action of LF and EF on cytoplasmic substrates (1, 2). Anthrax toxin intoxication is initiated by the binding of PA to either of two receptors, capillary morphogenesis protein-2 (CMG-2) or tumor endothelial marker-8 (TEM-8) (3, 4). Subsequently, PA is cleaved at the sequence, $^{164}$RKKR$^{167}$, by cell surface-localized furin or furin-like proprotein convertases (5). This endoproteolytic cleavage is absolutely required for toxin activation and triggers all subsequent steps of the intoxication process. The C-terminal 63-kDa fragment of PA (PA63) remains bound to the cell surface after endoproteolytic cleavage and undergoes a conformational change that leads to the formation of a PA63 heptamer or octamer that subsequently binds up to four molecules of LF or EF with high affinity (6, 7). The complex of PA63 and LF or EF is then endocytosed, and PA63 undergoes pH-induced conformational changes in the endosomal/lysosomal compartment to form a channel that facilitates the unfolding and translocation of LF and EF to the cytoplasm. EF is an adenylate cyclase proposed to lead to the formation of supraphysiological intracellular levels of cyclic AMP (8). LF is a zinc-dependent metalloproteinase that can cleave and inactivate several mitogen-activated protein kinase kinases, NLR family pyrin domain containing 1 (NLRP1), and regulatory subunits of phosphoinositide-3 kinase (PI3K)-p85α (PIK3R1) and p85β

‡ These authors contributed equally to this research.
* For correspondence: Thomas H. Bugge, thomas.bugge@nih.gov.

(PIK3R2) (9–11). Although required for intoxication, the cellular distribution of CMG-2 and TEM-8 and the function of each receptor in the intoxication in specific organs remain to be fully elucidated. Notably, assays for direct visualization of anthrax toxin intoxication *in vivo* are not available, and the tissue and cellular targets for anthrax toxin during *in vivo* infection have been inferred only indirectly from analysis of tissues from intoxicated animals or from biochemical and genetic analysis of anthrax toxin targets (12, 13).

LF is stable in circulation when administered alone and only becomes cell surface-associated after the binding of PA to CMG-2 or TEM-8 and its subsequent proteolytic cleavage to PA63. It has long been noted that LF residues 1 to 254 suffice to achieve translocation of a variety of "passenger" polypeptides and other molecules into the cytoplasm of the cells in a PA63-dependent manner (14, 15). These include other bacterial toxins and bacterial proteins (14, 16–20), fluorescent proteins (21), viral proteins (22–25), eukaryotic proteins (26–29), and radioisotopes (30, 31). Thus, the fusion or conjugation of LF to imageable moieties could provide ideal agents for studying the cellular intoxication by anthrax toxin *in vivo*. A significant caveat to this approach, however, is the low number of LF molecules successfully translocated to the cytoplasm through the PA pore, which makes most imaging modalities poorly suited to study anthrax toxin intoxication in whole-animal systems (19, 28). A second challenge to whole-animal imaging approaches is that most imaging modalities, such as radionuclides, enzymes such as horseradish peroxidase and β-galactosidase, and fluorescent proteins, likely would not discriminate between productive intoxication (*i.e.*, PA-dependent entry into the cytoplasm) and nonproductive interactions of the labeled toxin with cells, such as cell surface retention, fluid phase pinocytosis, and endosomal/lysosomal accumulation of intact or partially degraded toxin conjugates.

Spleen extracts from reporter mice carrying a Cre-activated β-galactosidase transgene have been shown to express increased β-galactosidase activity when infected with *Salmonella enterica* serovar Typhimurium carrying the type III secreted protein, SopE, fused to bacteriophage P1 Cre recombinase (32). Although single-cell resolution was not achieved, presumably due to a low number of cells being infected (32), the study provided evidence that bacterial protein-Cre fusion proteins may display sufficient enzymatic activity in animals to induce LoxP-dependent recombination.

In this study, we used a combined biochemical and genetic approach to image anthrax toxin intoxication in animals. Specifically, we generated a tripartite fusion protein that consists of the N-terminal domain of LF fused to a nuclear localization signal-tagged bacteriophage P1 Cre recombinase (LFn-NLS-Cre). When PA and LFn-NLS-Cre were coadministered to transgenic mice that ubiquitously express a red fluorescent protein (tdTomato) in the absence of Cre activity and a green fluorescent protein (eGFP) in the presence of Cre activity (hereafter *mTmG* mice), anthrax toxin intoxication could readily be visualized at single-cell resolution by using confocal microscopy of unfixed and unprocessed organs or by flow cytometry. By superimposing individual or combined genetic deficiency of either TEM-8 or CMG-2 in *mTmG* mice, we were able to directly establish the importance of each receptor in anthrax toxin intoxication in individual tissues.

The assay presented here should be useful for basic and clinical/translational studies of *Bacillus anthracis* infection, and it may be easily adapted to image intoxication in animals by related bacterial type III toxins. Furthermore, the assay will be valuable for identifying on- and off-targets for reengineered anthrax toxins currently in clinical and preclinical development for the treatment of solid tumors (33–48). When used in conjunction with modified PA variants that are activated by specific cell surface proteases, the assay may also be suitable for *in vivo* imaging of specific cell surface proteolytic activity in a variety of physiological and pathological processes.

## Results

### Generation of LFn-Cre recombinase fusion proteins capable of PA-dependent cytoplasmic translocation

We have previously shown that PA-dependent translocation of a LF-β-lactamase fusion protein can be imaged in cultured cells by using a cell-penetrating β-lactamase quenched fluorescence resonance energy transfer substrate (19). The adaptation of this assay for imaging anthrax toxin intoxication in whole animals, while hypothetically feasible, is prohibited by the high cost of the β-lactamase substrate and, likely, by logistic problems associated with systemic delivery of the substrate to animals. We therefore explored the possibility of combining biochemical and genetic approaches to imaging anthrax toxin intoxication in whole animals. Specifically, we generated a series of proteins that consist of the PA-binding domain of LF (LFn) either fused directly to the bacteriophage P1 Cre recombinase (LFn-Cre) or linked *via* a nuclear localization signal (LFn-NLS-Cre), a native ubiquitin protein (LFn-native ubiquitin-NLS-Cre), or a modified ubiquitin protein followed by a nuclear localization signal (LFn-modified ubiquitin-NLS-Cre) in which the seven Lys residues of ubiquitin are replaced with Arg. This modified ubiquitin also contains the substitutions V5A and V17A chosen to destabilize the N-terminal region and facilitate translocation through the PA channel (Fig. 1, *A* and *B*). The inclusion of ubiquitin as a linker was based on the expectation that ubiquitin fusions of this type, once delivered to the cytosol, would be cleaved by deubiquitinating enzymes, releasing the Cre domain as a smaller entity that may have greater access to the nucleus, the location of its target DNA substrate (49). Furthermore, release from LFn could decrease the probability that ubiquitination of the LFn region would deliver the entire fusion protein to the proteasome for degradation. Similarly, the replacement of the seven Lys residues of ubiquitin with Arg in LFn-modified ubiquitin NLS-Cre could limit ubiquitination and increase stability.

Preliminary testing of the four purified LFn-Cre proteins was done in CV1-5B reporter cells, which contain a Cre-activated β-galactosidase gene, by treating the cells with increasing concentrations of fusion protein in the presence of a fixed concentration of PA (Fig. 1, *C–E*). These experiments identified LFn-NLS-Cre as the most effective of the four fusion proteins.

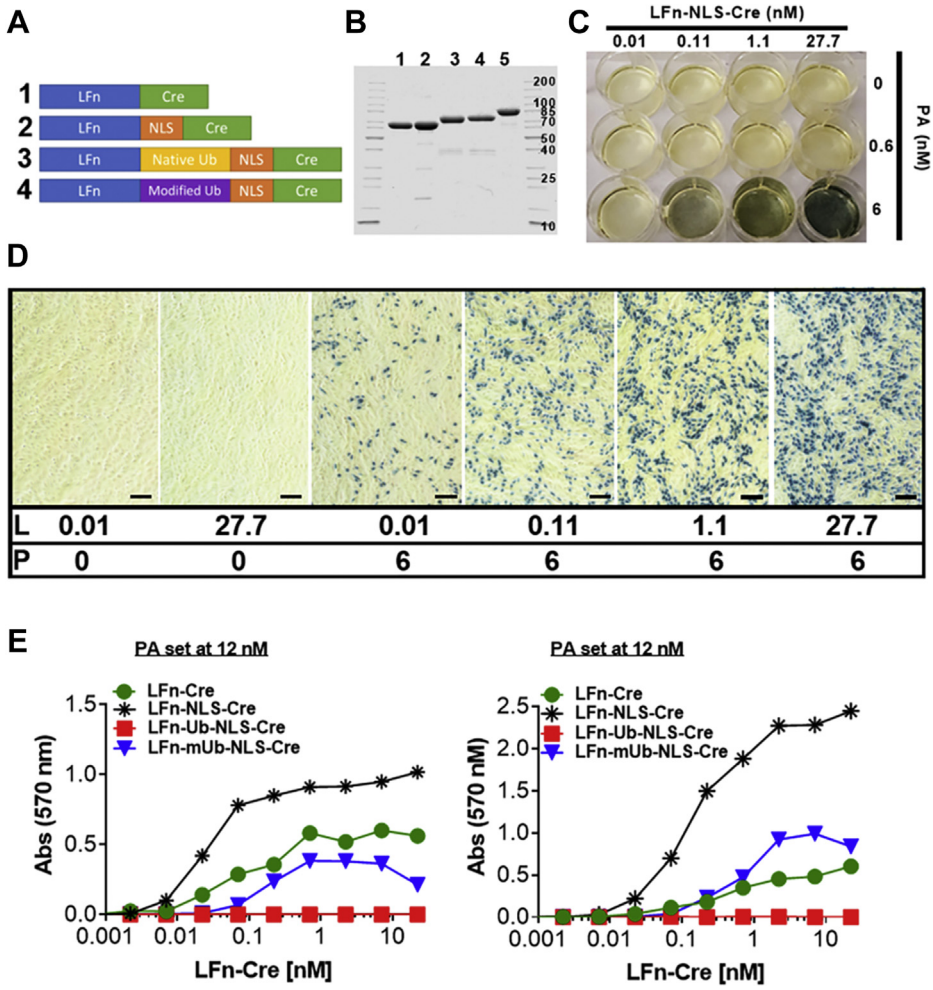


**Figure 1. Generation of LFn-Cre fusion proteins capable of PA-dependent cellular entry.** *A*, schematic structure of LFn-Cre (1), LFn-NLS-Cre (2), LFn-native ubiquitin-NLS-Cre (3), and LFn-modified ubiquitin-NLS-Cre (4) fusion proteins. *B*, Coomassie gel showing the purified proteins corresponding to constructs in (*A*). Lane 5 is the PA preparation used in all experiments. Only select molecular weight marker bands (kDa) are indicated due to space limitations. *C* and *D*, CV1-5B cells harboring a single copy of lox-stop-lox (Cre-activated) β-galactosidase gene were incubated with varying concentrations of LFn-NLS-Cre and PA as indicated for 40 h. Cells were then stained *in situ* for β-galactosidase activity using the chromogenic substrate, 5-bromo-3-indolyl β-D-galactopyranoside (Bluo-Gal) as described in Experimental procedures. In panel *D*, L is LFn-NLS-Cre and P is PA. Numbers are the nanomolar concentration of each component. Images collected with 10× objective. Scale bar is 100 μm. *E*, CV1-5B cells were plated at low density (*left panel*) or high density (*right panel*) and incubated with increasing concentrations of LFn-NLS-Cre, LFn-Cre, LFn-native ubiquitin-NLS-Cre, or LFn-modified ubiquitin-NLS-Cre fusion proteins in the presence of 12 nM PA. Cells were stained for β-galactosidase activity after 40 h using chlorophenol red-β-D-galactopyranoside (CPRG), as described in Experimental procedures. LFn-NLS-Cre, LF fused to a nuclear localization signal-tagged Cre recombinase; PA, protective antigen.

The need for an NLS, the only feature present in LFn-NLS-Cre compared with LFn-Cre (Fig. 1*A*), suggests that the NLS reported to exist in Cre (50) is not by itself sufficient to maximize nuclear delivery in this context. The alternative explanation that the added NLS in LFn-NLS-Cre provides a target by which cytosolic proteases release the Cre domain cannot be discounted without further study. The total inactivity of LFn-native ubiquitin-NLS-Cre compared with that of LFn-modified ubiquitin-NLS-Cre indicated that native ubiquitin is unable to translocate through the PA pore. The entry of LFn-NLS-Cre into cells was highly PA-dependent, with very few CV1-5B cells displaying β-galactosidase activity in the absence of PA, even at high concentrations of the fusion protein (Fig. 1*D*).

### *Imaging anthrax toxin intoxication in mice*

The above studies showed that LFn-Cre fusion proteins could translocate to the cytoplasm in a PA-dependent manner that the Cre moiety (alone or as an intact fusion protein) thereafter was imported to the nucleus, and that it retained its recombinase activity after nuclear translocation. This indicated that LFn-Cre fusion proteins, when used in conjunction with appropriate transgenic mouse Cre reporter strains, could be suitable for imaging anthrax toxin intoxication *in vivo*. The B6.129(Cg)-*Gt(ROSA)26Sortm4(ACTB-tdTomato,-EGFP)Luo*/J transgenic mouse (hereafter *mTmG*) is a widely used reporter strain for Cre activity (51). The strain constitutively expresses a floxed plasma membrane-tagged tdTomato (mTomato) fluorescent protein gene under the control of a cytomegalovirus-β-actin enhancer-promoter. This gene is excised by Cre, which simultaneously allows for transcription of a plasma membrane-tagged enhanced green fluorescent protein (eGFP)-expressing gene by placing it proximal to the cytomegalovirus-β-actin enhancer-promoter (Fig. 2*A*). Thus, following cytoplasmic translocation of LFn-NLS-Cre through the PA pore and subsequent nuclear

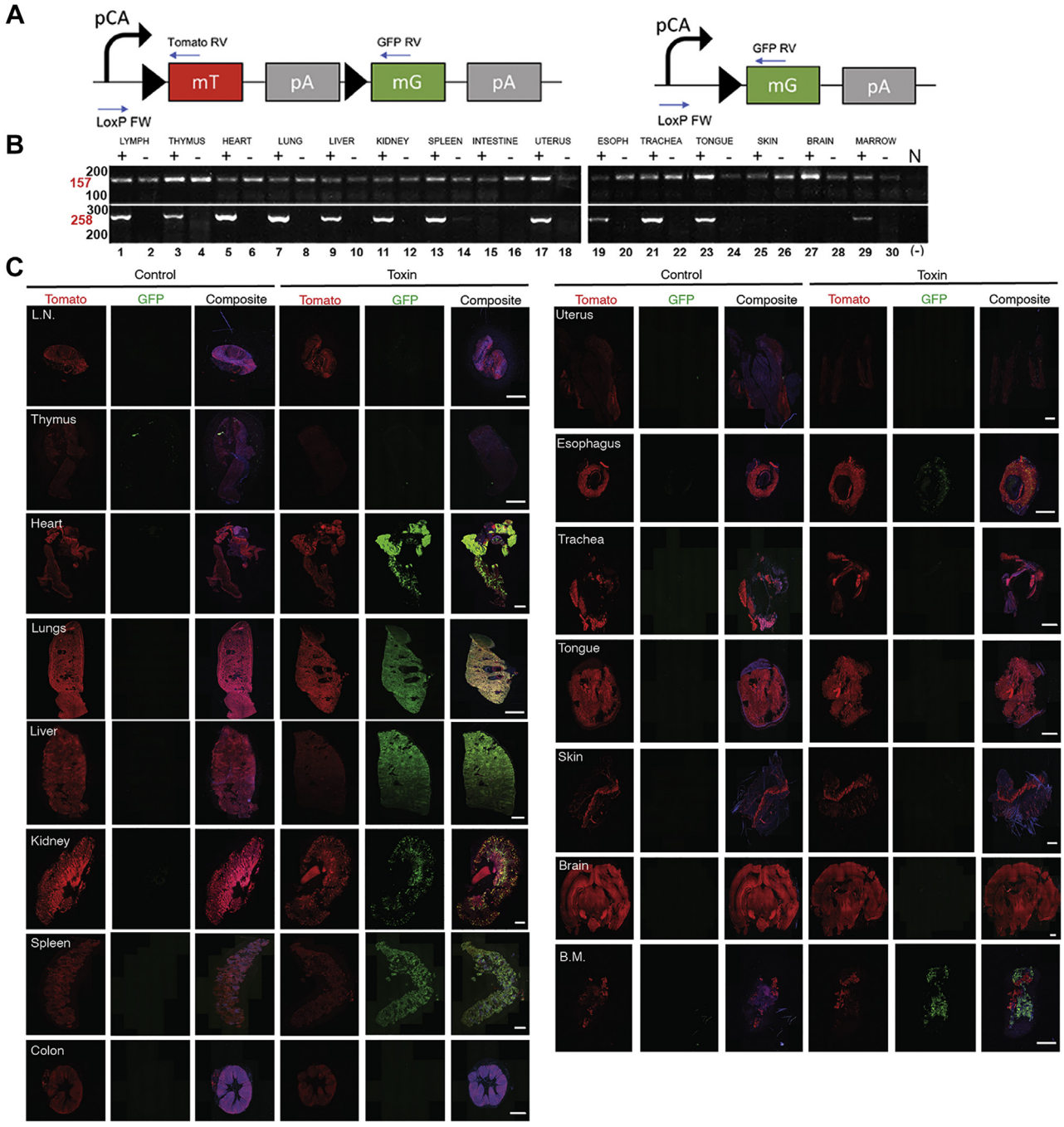


**Figure 2. Analysis of LFn-NLS-Cre activity in toxin-injected *mTmG*$^{+/0}$ mice by PCR and by whole organ imaging.** *A*, schematic depiction of *mTmG* transgene prior to (*left*) and after (*right*) Cre-mediated recombination. The locations of primers used for detection of the non-recombined allele (LoxP FW and Tomato RV, generating a 157 bp PCR product) and recombined allele (LoxP FW and GFP RV, generating a 258 bp PCR product) are indicated with *straight blue arrows*. The locations of the transcription initiation site (*curved arrow*), LoxP sites (*black triangles*), mTomato (mT) and eGFP (mG) genes, and poly A sites (pA) are shown. *B*, ethidium bromide-stained agarose gels of PCR products generated from DNA isolated from the lymph nodes (LYMPH, lanes 1 and 2), thymus (lanes 3 and 4), heart (lanes 5 and 6), lungs (lanes 7 and 8), liver (lanes 9 and 10), kidney (lanes 11 and 12), spleen (lanes 13 and 14), intestine (lanes 15 and 16), uterus (lanes 17 and 18), esophagus (ESOPH, lanes 19 and 20), trachea (lanes 21 and 22), tongue (lanes 23 and 24), skin (lanes 25 and 26), brain (lanes 27 and 28), and bone marrow (MARROW) (lanes 29 and 30) of an *mTmG*$^{+/0}$ mouse injected with 25 μg LFn-NLS-Cre and 25 μg PA (lanes 1, 3, 5, 7, 9, 11, 13, 15, 17, 19, 21, 23, 25, 27, and 29) or a non-injected *mTmG*$^{+/0}$ littermate (lanes 2, 4, 6, 8, 10, 12, 14, 16, 18, 20, 22, 24, 26, 28, and 30). Positions of PCR products generated from nonrecombined (157 bp) and recombined (258 bp) *mTmG* alleles are shown at *left* in *red* types. Positions of molecular weight markers (100 and 200 bp for *top panel* and 200 and 300 bp for *bottom panel*) are shown at *left*. *C*, low-magnification confocal images of fresh slices of (*top* to *bottom*) the lymph node (L.N.), thymus, heart, lungs, liver, kidney, spleen, intestine (colon), uterus, esophagus, trachea, tongue, skin, brain, and bone marrow (B.M.) from *mTmG*$^{+/0}$ mice intravenously injected with PBS at 0 h, 24 h, 48 h, 72 h, and 96 h with analysis at 120 h (*left three panels*, Control) or with 25 μg LFn-NLS-Cre and PA at 0 h, 24 h, 48 h, 72 h, and 96 h with analysis at 120 h (*right three panels*, Toxin). The images were collected using a 20× objective. The whole organ images were assembled from individual images and were stitched together to cover the entire organ slice. Nuclei (*blue*) were visualized by systemic Hoechst administration to the mice prior to analysis. Separated *red* (Tomato), *green* (GFP), and composite *red*, *green*, and *blue* (Composite) channels are shown for each organ. Size bars: 1 mm. LFn-NLS-Cre, LF fused to a nuclear localization signal-tagged Cre recombinase; N, no DNA.

import, intoxicated cells should display green fluorescent plasma membranes, while plasma membranes of non-intoxicated cells should display only red fluorescence.

To test if PA and LFn-NLS-Cre could mediate LoxP-dependent recombination in a whole-animal context, we first designed PCR primer sets that would selectively amplify, respectively, the nonrecombined and the recombined *mTmG* transgene (Fig. 2*A*). Interestingly, a PCR product derived from the recombined transgene was readily detected in the heart, lungs, liver, kidney, spleen, lymph nodes, thymus, uterus, esophagus, trachea, tongue, and bone marrow of $mTmG^{+/0}$ mice injected with LFn-NLS-Cre and PA but not in these organs from noninjected $mTmG^{+/0}$ mice (Fig. 2*B*). This PCR product was not observed in the intestine, skin, and brain of mice injected with LFn-NLS-Cre and PA (Fig. 2*B*).

We next determined the ability to detect fluorescence in $mTmG^{+/0}$ mice by confocal microscopy of unfixed whole organ slices, which could serve as a convenient readout for Cre activity. Wild-type mice were analyzed in parallel as a control for autofluorescence. To obtain semiquantitative estimates of fluorescence intensities of the examined organs, in this and the following experiments, we generated composite images of the entire organ slice from confocal images acquired at low magnification. As expected, red fluorescence of variable intensity was observed in multiple organs of $mTmG^{+/0}$ mice but not in the corresponding organs from wild-type mice imaged using the identical conditions (Fig. S2). This indicated that the *mTmG* mouse strain should be suitable for the detection of anthrax toxin intoxication in cells in a variety of organs and tissues by this simple procedure.

Having established that fluorescence in $mTmG^{+/0}$ mice can readily be detected by confocal microscopy of unfixed whole organ slices, we next intravenously injected $mTmG^{+/0}$ and wild-type mice with LFn-NLS-Cre alone, PA alone, or with PA in combination with LFn-NLS-Cre (Fig. S3). Mice were killed 24 h later, and slices of excised organs were immediately examined by confocal microscopy. Organs from $mTmG^{+/0}$ mice injected with LFn-NLS-Cre alone displayed only red fluorescence (Fig. S3, *A*, *A'*, *D*, *D'*, *G*, *G'*, *J*, *J'*, *M* and *M'*), importantly showing that the LFn-NLS-Cre protein by itself does not gain access to cells. As expected, organs from mice injected with PA alone also displayed only red fluorescence (Fig. S3, *B*, *B'*, *E*, *E'*, *H*, *H'*, *K*, *K'*, *N* and *N'*). Interestingly, however, when analyzing these organs from $mTmG^{+/0}$ mice injected with LFn-NLS-Cre in combination with PA, both red (Fig. S3, *C*, *F*, *I*, *L* and *O*) and green fluorescence were readily detected in the heart, kidney, liver, lungs, and spleen (Fig. S3, *C'*, *F'*, *I'*, *L'* and *O'*), indicating that PA-dependent translocation of LFn-NLS-Cre to the cytoplasm of cells in these organs takes place and that the subsequent nuclear import of the fusion protein leads to the excision of the floxed mTomato gene. No green fluorescence was observed in the same organs of wild-type mice injected with LFn-NLS-Cre in combination with PA, further demonstrating the origin of the green fluorescent signal from *de novo* expression of eGFP (Fig. S4, compare *A* with *B*, *C* with *D*, *E* with *F*, *G* with *H*, *I* with *J*). Compatible with the PCR analysis, green fluorescence was weak or absent in the intestine (Fig. S5, *A* and *B*), skin (Fig. S5, *C* and *D*), and brain (Fig. S5, *E* and *F*) slices, although cells in these organs of $mTmG^{+/0}$ mice were previously shown to undergo recombination *in vivo* and express eGFP in the presence of a Cre-expressing transgene (51).

### Effect of route of administration, dose, and time of analysis on imaging of intoxication

Parameters affecting the intoxication process and the optimal use of mTomato/eGFP fluorescence as a readout for anthrax toxin intoxication would be expected to include the mode and dose of toxin delivery, tissue accessibility, receptor expression, efficiency of cytoplasmic translocation and nuclear transport of the LFn-NLS-Cre fusion protein, rate of Cre-mediated recombination, decay rate of the mTomato mRNA and protein, the rate of transcription, translation and attainment of steady state levels of the eGFP protein, ploidy of the target cells (diploid *versus* polyploid, carrying one or more than one transgene), and time of imaging after toxin administration. The next set of experiments were aimed at empirically addressing some of these issues by varying the mode and dose of toxin delivery, number of injections, and time from injection to imaging. We first compared low-magnification confocal images of green fluorescence obtained from whole organ slices of the heart, kidney, liver, lungs, and spleen from $mTmG^{+/0}$ mice injected either intravenously or intraperitoneally with PA in combination with LFn-NLS-Cre (Fig. S6). This analysis showed that toxin administered intraperitoneally intoxicated the organs less efficiently, as evidenced by less green fluorescence, than when administered intravenously (Fig. S6, compare *A*–*C* with *D*, *E*–*G* with *H*, *I*–*K* with *L*, *M*–*O* with *P*, *Q*–*S* with *T*).

We next studied the effect of multiple injections of PA and LFn-NLS-Cre on the intoxication in the five organs analyzed above (Fig. S7). Specifically, we injected $mTmG^{+/0}$ mice with PA and LFn-NLS-Cre at 0 h, 24 h, 48 h, and 72 h and procured low-magnification red and green confocal fluorescence images of organ slices at 24 h, 48 h, 72 h, and 120 h. For each time point analyzed, a separate control group of mice injected with PA and LFn-NLS-Cre once at 0 h was included to control for Cre-mediated recombination occurring during the assay period and/or the eGFP protein not having attained steady-state levels at 24 h. This control experiment, indeed, showed that the eGFP signal in organs of mice having received a single injection of PA and LFn-NLS-Cre increased qualitatively beyond 24 h, with the possible exception of the liver (Fig. S7, compare *A'* with *B'*, *C'*, and *D'*, *E'* with *F'*, *G'*, and *H'*, *I'* with *J'*, *K'*, and *L'*, *M'* with *N'*, *O'*, and *P'*, *Q'* with *R'*, *S'*, and *T'*). However, for the kidney (Fig. S7, compare *F'* with *F'''*, *G'* with *G'''*, *H'* with *H'''*), liver (Fig. S7, compare *J'* with *J'''*, *K'* with *K'''*, *L'* with *L'''*), and spleen (Fig. S7, compare *R'* with *R'''*, *S'* with *S'''*, *T'* with *T'''*), an increased eGFP signal was evident in mice receiving multiple injections of PA and LFn-NLS-Cre, as compared with single-injected control mice. Interestingly, the mTomato signal in the liver was greatly diminished already at 48 h in mice receiving either single or multiple injections of PA

and LFn-NLS-Cre (Fig. S7, compare *I* with *J* and *J''*). This indicates that intoxication in the majority of cells in this organ was achieved.

To examine the effect of the dose of toxin administered on intoxication, we injected $mTmG^{+/0}$ mice with 5, 15, and 25 μg PA and LFn-NLS-Cre and imaged their organs 24 h later. At the 5 μg dose, only the lungs displayed a faint eGFP signal (Fig. S8*J'*). At the 15 μg dose, eGFP signals were seen in the liver (Fig. S8*H'*) and lungs (Fig. S8*K'*). At the 25 μg toxin dose, an eGFP signal also became evident in the heart (Fig. S8*C'*), kidney (Fig. S8*F'*), and spleen (Fig. S8*O'*).

To determine when an eGFP signal is first detectable after the administration of PA and LFn-NLS-Cre, we injected $mTmG^{+/0}$ mice with 75 μg of each protein and examined the heart, kidney, liver, lungs, and spleen by confocal microscopy at 6, 8, 10, and 12 h (Fig. S9). Whereas no signal was observed at any of these time points in the heart (Fig. S9, *A'*, *B'*, *C'* and *D'*), kidney (Fig. S9, *E'*, *F'*, *G'* and *H'*), lungs (Fig. S9, *M'*, *N'*, *O'* and *P'*), and spleen (Fig. S9, *Q'*, *R'*, *S'* and *T'*), faint eGFP signals were observed in the liver at 12 h (Fig. S9*L'*).

We next surveyed a wide range of organs for anthrax toxin intoxication by intravenously injecting $mTmG^{+/0}$ mice at 0 h, 24 h, 48 h, and 72 h with either PBS or 25 μg LFn-NLS-Cre and 25 μg PA, followed by analysis of tissues by confocal microscopy at 120 h (Fig. 2*C*). As found in the prior experiments, intoxication was easily detected in the heart, lung, liver, kidney, and spleen. In addition, intoxication was observed in the esophagus and bone marrow, whereas intoxication of the lymph nodes, thymus, intestine, uterus, trachea, tongue, skin, and brain was not observed.

### *High-resolution imaging of anthrax toxin intoxication*

Using the knowledge gained from the above experiments, we next tested the ability of the assay to image intoxication in individual cells in unprocessed organs. For this purpose, mice received three intravenous injections of 25 μg LFn-NLS-Cre and 25 μg PA at 0 h, 24 h, and 48 h. Seventy-two hours after the first injection, confocal images of blue (nuclei), red (tdTomato), and green (eGFP) fluorescence of slices of the heart, kidney, liver, lungs, and spleen were acquired at high magnification (Fig. 3). This analysis showed that in tissues of these five organs, nonintoxicated and intoxicated individual cells were readily distinguishable by their red and their green membrane-confined fluorescence, respectively.

### *Effect of genetic elimination of CMG-2 and TEM-8 on anthrax toxin intoxication*

We next interbred previously generated CMG-2-deficient ($Cmg2^{-/-}$) and TEM-8-deficient ($Tem8^{-/-}$) mice to $mTmG^{+/0}$ mice to generate, respectively, $Cmg2^{-/-}$;$mTmG^{+/0}$ and $Tem8^{-/-}$;$mTmG^{+/0}$ mice. These mice, together with $mTmG^{+/0}$

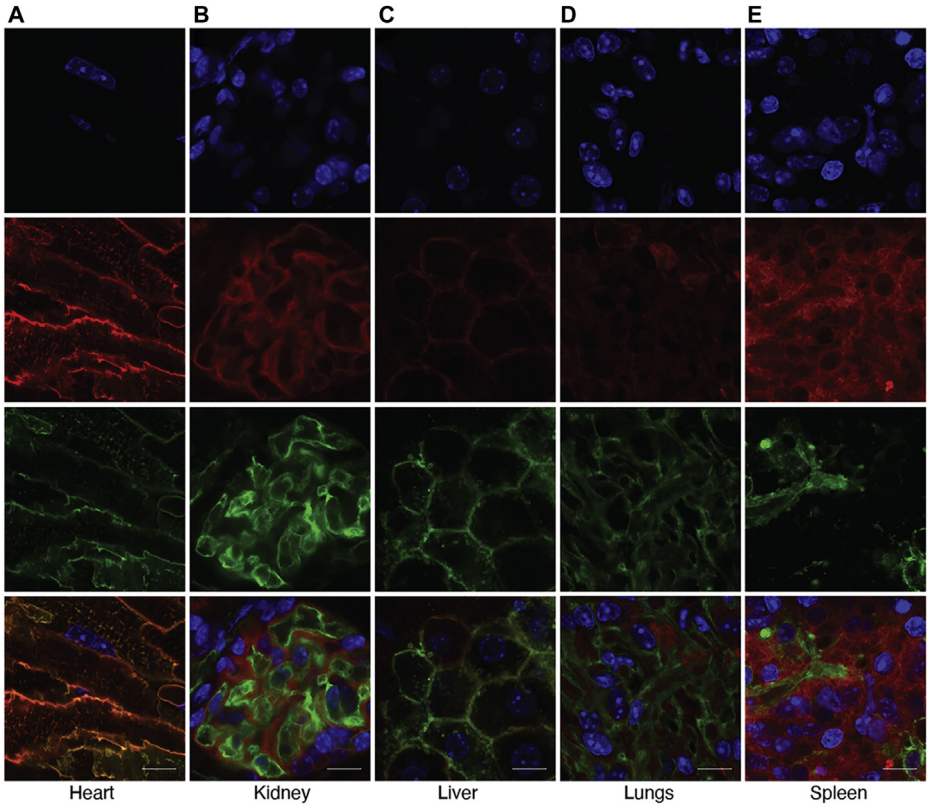


**Figure 3. Imaging of anthrax toxin intoxication of individual cells.** High-magnification confocal images of slices of the heart (column *A*), kidney (column *B*), liver (column *C*), lungs (column *D*), and spleen (column *E*) from $mTmG^{+/0}$ mice after intravenous administration of 25 μg LFn-NLS-Cre and 25 μg PA at 0 h, 24 h, and 48 h with analysis at 72 h. *Top row*, nuclei (blue fluorescence) visualized by Hoechst administration to the mice prior to analysis. *Second row from top*, tdTomato (red fluorescence). *Second row from bottom*, membrane-associated eGFP (green fluorescence). *Bottom row*, composite images of Hoechst, tdTomato, and eGFP fluorescence. The images were collected using a 60× objective. Size bars: 10 μm.

mice, were injected at 0 h, 24 h, 48 h, and 72 h with 25 μg LFn-NLS-Cre and 25 μg PA, and red, green, and blue (nuclei) confocal fluorescence images of organ slices from the heart, kidney, liver, lungs, and spleen were acquired at 120 h. This injection scheme, as expected from the preceding experiments, resulted in green fluorescence of cells from the heart, liver and lungs, kidney, and spleen of *mTmG*$^{+/0}$ mice (Fig. 4, *A–A‴*, *C–C‴*, *E–E‴*, *G–G‴* and *I–I‴*). In sharp contrast, green fluorescent cells were essentially absent in the heart and liver of *Cmg2*$^{-/-}$;*mTmG*$^{+}$ mice, showing that CMG-2 mediates intoxication in these organs uncompensated by TEM-8 (Fig. 4, *B–B‴* and *F–F‴*). The pattern of fluorescence in the kidney, lungs, and spleen was not appreciably different between *mTmG*$^{+}$ and *Cmg2*$^{-/-}$;*mTmG*$^{+}$ mice (Fig. 4, *D–D‴*, *H–H‴* and *J–J‴*).

We next performed a similar comparison of toxin-treated *mTmG*$^{+}$ and *Tem8*$^{-/-}$;*mTmG*$^{+}$ mice analyzed in parallel. This showed that, unlike CMG-2, TEM-8 was not critical for the intoxication of the heart and liver (Fig. 5, *B–B‴* and *F–F‴*), revealing CMG-2 as the dominant receptor for the intoxication in these organs. Intoxication in the lungs was not substantially affected by the loss of TEM-8 (Fig. 5, *H–H‴*), suggesting that intoxication in this organ is mediated by either of the two anthrax toxin receptors. In sharp contrast, the loss

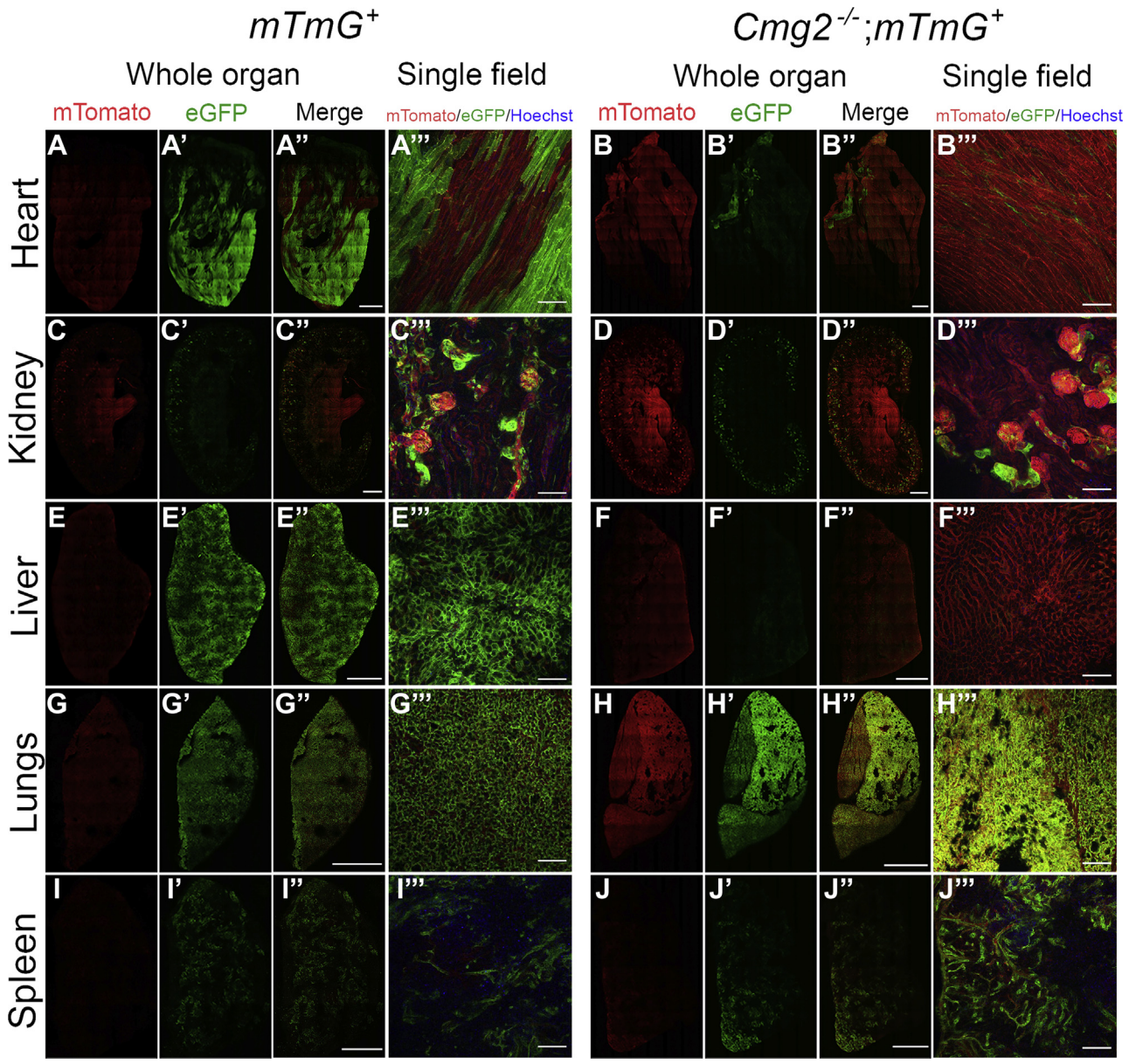


**Figure 4. CMG-2 is critical for anthrax toxin intoxication in the heart and liver.** Low-magnification confocal images of fresh slices of the heart (*A–A‴* and *B–B‴*), kidney (*C–C‴* and *D–D‴*), liver (*E–E‴* and *F–F‴*), lungs (*G–G‴* and *H–H‴*), and spleen (*I–I‴* and *J–J‴*) from CMG-2-sufficient, *mTmG*-sufficient (*left panel*) and CMG-2-deficient, *mTmG*-sufficient (*right panel*) mice after intravenous administrations of 25 μg LFn-NLS-Cre and PA at 0 h, 24 h, 48 h, 72 h, and 96 h with analysis at 120 h. The images were collected using a 20× objective. The whole organ images were assembled from individual images and were stitched together to cover the entire organ slice. Nuclei (*blue*) were visualized by systemic Hoechst administration to the mice prior to analysis. Size bars for whole organ: 1 mm. Size bars for single field: 100 μm. The data are representative of four separate experiments. CMG-2, capillary morphogenesis protein-2.

of TEM-8 markedly reduced the green fluorescent signal in the kidney (Fig. 5, *D–D‴*) and in trabecular structures of the spleen (Fig. 5, *J–J‴*), suggesting that TEM-8 plays a key role in the intoxication in these organs. Neither green nor red fluorescence was observable in areas of the spleen harboring leukocytes. However, both nonintoxicated, red fluorescent and intoxicated green fluorescent spleen leukocytes were readily detected by flow cytometry (see below).

The above studies revealed minimal effect of individual deficiencies in either CMG-2 or TEM-8 on the intoxication of lungs. To exclude that this was a consequence of hitherto unrecognized anthrax toxin receptors, we imaged intoxication of *Cmg2*$^{-/-}$;*Tem8*$^{-/-}$;*mTmG*$^{+}$ mice (Fig. 6). This analysis showed that the combined elimination of CMG-2 and TEM-8 completely prevented intoxication of all tissues examined.

To determine the role of TEM-8 and CMG-2 in intoxication of leukocytes, single-cell suspensions of CD45-positive leukocytes from spleens were analyzed by flow cytometry. About half of leukocytes from *mTmG*$^{+}$ spleens displayed red fluorescence indicating expression of the transgene (Fig. 7*A*, left panel). Less than 2% of the leukocytes expressed green fluorescence, showing that intoxication of spleen leukocytes is inefficient (Fig. 7*A*, right panel). No significant reduction in the percentage of green fluorescent leukocytes was seen after elimination of TEM-8 (Fig. 7*A*, right panel). However, loss of CMG-2 resulted in a fivefold reduction in the percentage of

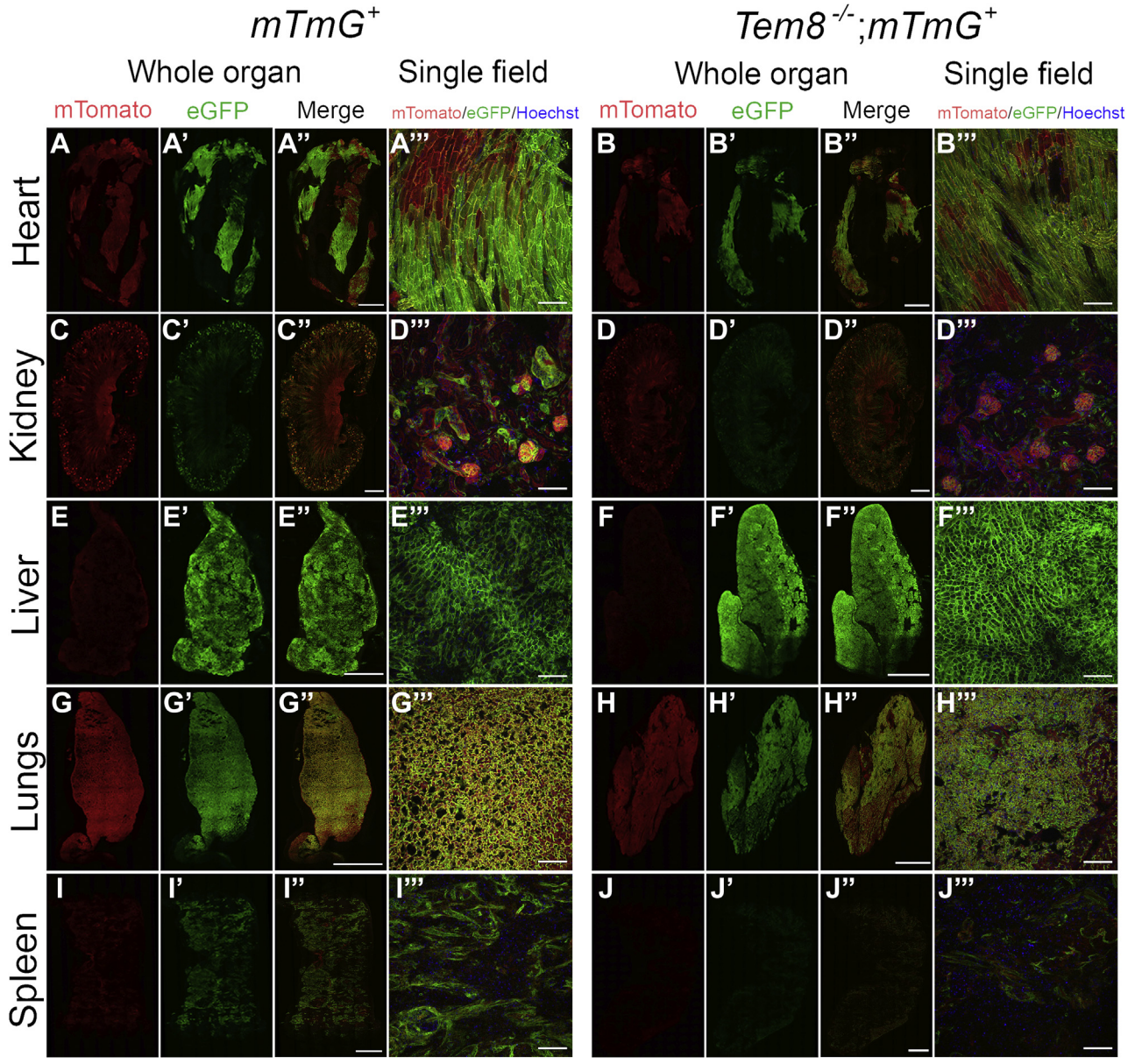


**Figure 5. TEM-8 has a key role in anthrax toxin intoxication in the kidney and spleen.** Low-magnification confocal images of fresh slices of the heart (*A–A‴* and *B–B‴*), kidney (*C–C‴* and *D–D‴*), liver (*E–E‴* and *F–F‴*), lungs (*G–G‴* and *H–H‴*), and spleen (*I–I‴* and *J–J‴*) from TEM-8-sufficient, *mTmG*-sufficient (*left panel*) and TEM-8-deficient, *mTmG*-sufficient (*right panel*) mice after intravenous administrations of 25 μg LFn-NLS-Cre and PA at 0 h, 24 h, 48 h, 72 h, and 96 h with analysis at 120 h. The images were collected using a 20× objective. The whole organ images were assembled from individual images and were stitched together to cover the entire organ slice. Nuclei (*blue*) were visualized by systemic Hoechst administration to the mice prior to analysis. Size bars for whole organ: 1 mm. Size bars for single field: 100 μm. The data are representative of four separate experiments. TEM-8, tumor endothelial marker-8.

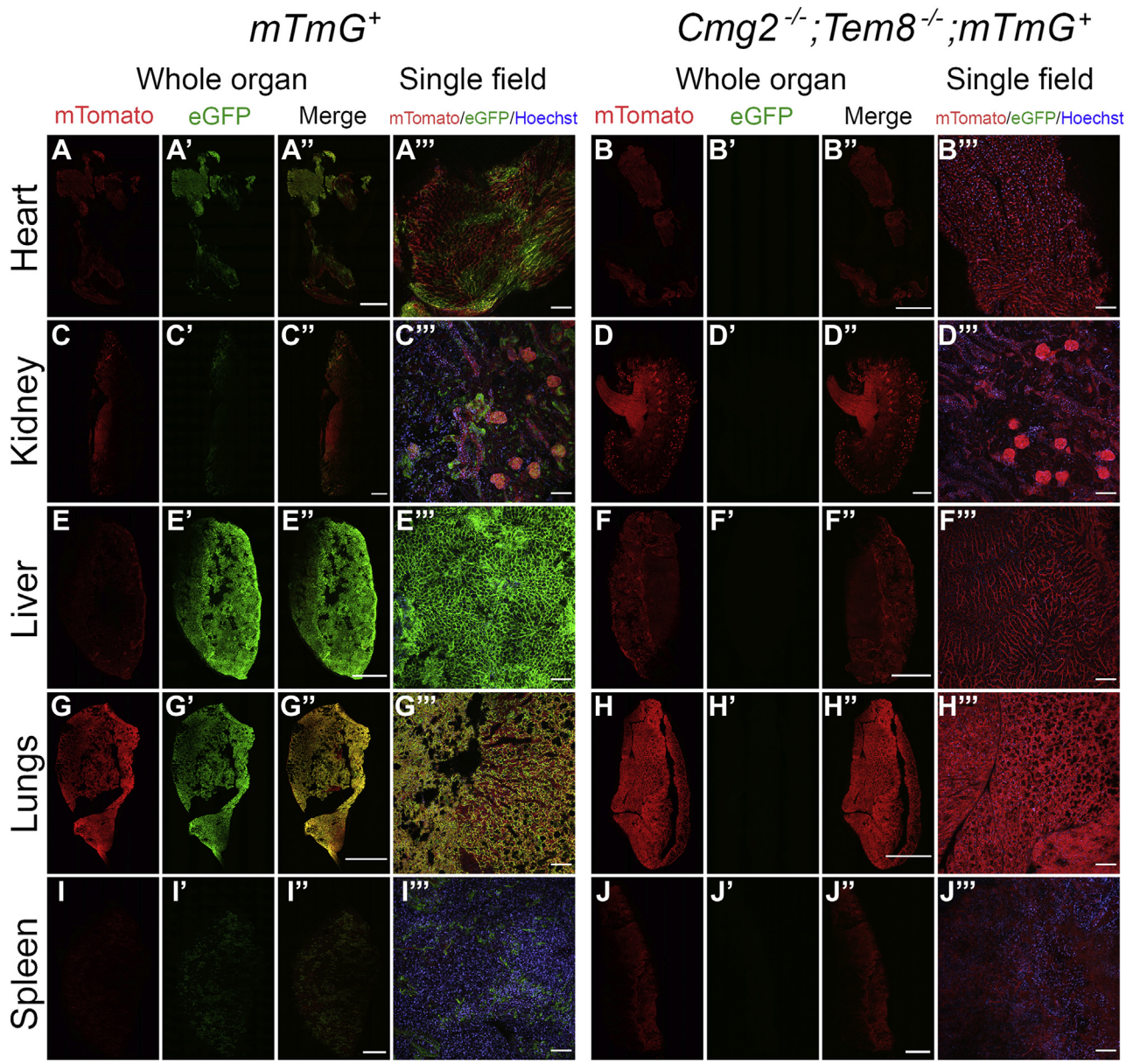


**Figure 6. Combined loss of CMG-2 and TEM-8 prevents anthrax toxin intoxication.** Low-magnification confocal images of fresh slices of the heart (*A–A‴* and *B–B‴*), kidney (*C–C‴* and *D–D‴*), liver (*E–E‴* and *F–F‴*), lungs (*G–G‴* and *H–H‴*), and spleen (*I–I‴* and *J–J‴*) from a CMG-2 and TEM-8-sufficient, *mTmG*-sufficient (*left panel*) and CMG-2 and TEM-8-deficient, *mTmG*-sufficient (*right panel*) mice after intravenous administrations of 25 μg LFn-NLS-Cre and PA at 0 h, 24 h, 48 h, 72 h, and 96 h with analysis at 120 h. The images were collected using a 20× objective. The whole organ images were assembled from individual images and were stitched together to cover the entire organ slice. Nuclei (*blue*) were visualized by systemic Hoechst administration to the mice prior to analysis. Size bars for whole organ: 1 mm. Size bars for single field: 100 μm. CMG-2, capillary morphogenesis protein-2; LFn-NLS-Cre, LF fused to a nuclear localization signal-tagged Cre recombinase; TEM-8, tumor endothelial marker-8.

green fluorescent leukocytes, revealing CMG-2 as the dominant receptor (Fig. 7*A*, right panel). When analyzing individual leukocyte subsets, this predominance of CMG-2 in intoxication was seen in B cells (Fig. 7*B*, red bars), T cells (Fig. 7*B*, yellow bars), neutrophils (Fig. 7*B*, green bars), and dendritic cells (Fig. 7*B*, blue bars), whereas monocytic cells were unaffected by single loss of either TEM-8 or CMG-2 (Fig. 7*B*, purple bars).

## Discussion

The ability to directly visualize the intoxication in cells by bacterial exotoxins in whole-animal systems is desirable in the context of enhancing the understanding of the pathogenesis of these toxins and exploring their uses as therapeutics. The development of such imaging assays is complicated by the often low numbers of toxin molecules targeting individual cells, making toxin detection challenging, as well as by the difficulty of providing sufficient spatial resolution to discriminate *bona-fide* intoxication from nonproductive association of the toxin with the target cell, such as cell surface retention or endosomal/lysosomal sequestration.

Here, we describe a novel assay that provides single-cell resolution imaging of anthrax toxin intoxication in animals. The assay takes advantage of the potential of genetic readout

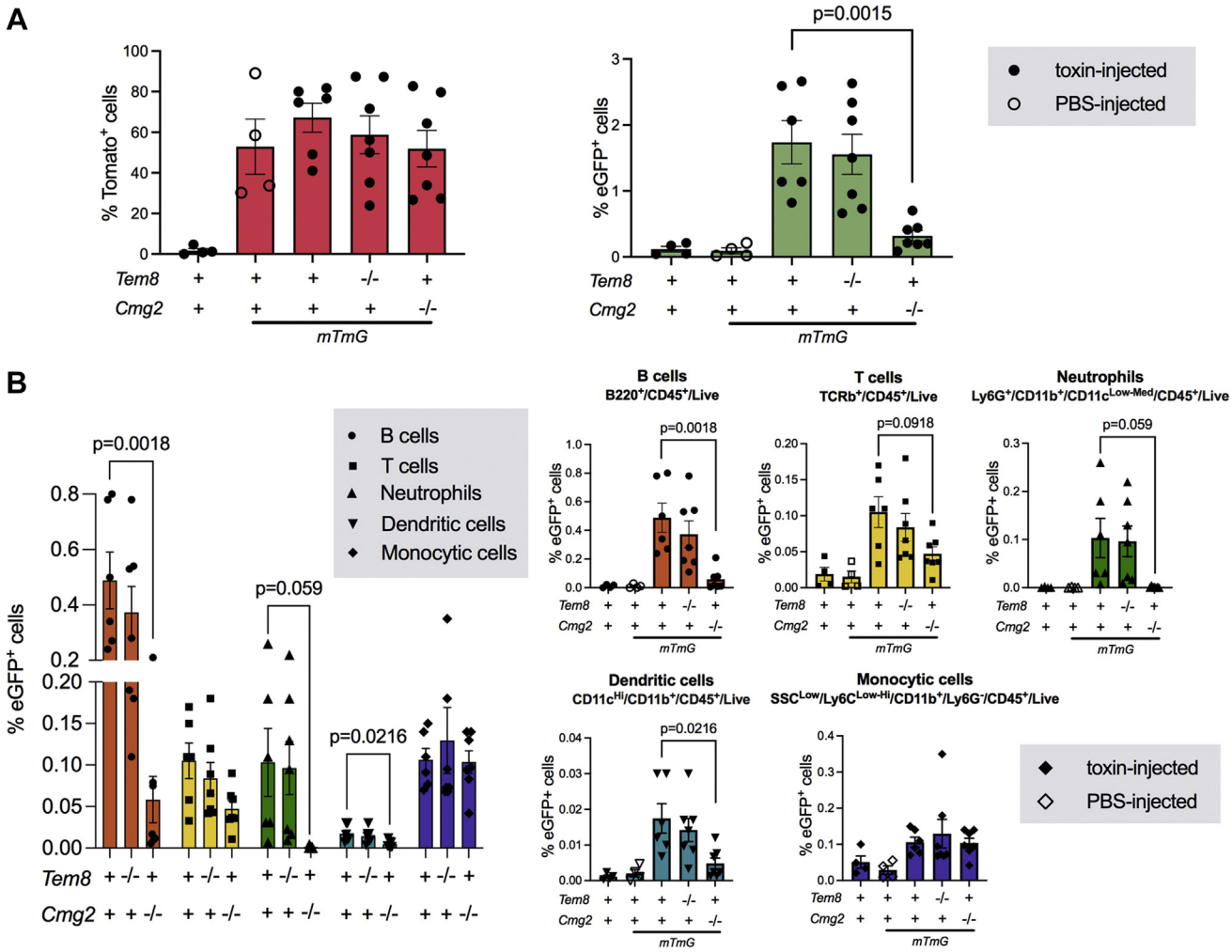


**Figure 7. Flow cytometry analysis of CMG-2 and TEM-8-dependent intoxication of spleen leukocytes.** Flow cytometric analysis of spleen leukocytes (CD45-positive cells) after intravenous administrations of 25 μg LFn-NLS-Cre and PA at 0 h, 24 h, 48 h, 72 h, and 96 h with analysis at 120 h. *A*, percent mTomato-positive (*left panel*) and eGFP-positive (*right panel*) leukocytes in toxin-injected wildtype, PBS-injected *mTmG* mice, toxin-injected *mTmG* mice, toxin-injected TEM-8-deficient *mTmG* mice, and toxin-injected CMG-2-deficient *mTmG* mice. *B*, effect of TEM-8 and CMG-2 deficiency on intoxication of B cells, T cells, neutrophils, dendritic cells, and monocytic cells. Mice were injected as above and analyzed by flow cytometry after staining with markers for each leukocyte sub-population. Results are shown as mean ± sem. *Left panel* shows compiled data from all leukocyte subsets. The remaining panels show individual data from each leukocyte subset in toxin-injected wild-type, PBS-injected *mTmG* mice, toxin-injected *mTmG* mice, toxin-injected TEM-8-deficient *mTmG* mice, and toxin-injected CMG-2-deficient *mTmG* mice. Data are compiled from four separate experiments with 4 to 7 mice per treatment group and genotype. CMG-2, capillary morphogenesis protein-2; LFn-NLS-Cre, LF fused to a nuclear localization signal-tagged Cre recombinase; TEM-8, tumor endothelial marker-8.

systems to provide near-unlimited signal amplification, in this case, entailing the activation of a fluorescent reporter gene by an anthrax toxin lethal factor-Cre fusion protein that is translocated to the cytoplasm through the anthrax protective antigen heptamer or octamer pore and subsequently imported to the nucleus. Intoxication in some organs could be detected as early as 12 h after systemic introduction of the toxin, and as expected, the efficiency of intoxication varied with toxin dose and mode of administration. The plasma membrane illumination provided by the membrane-targeted eGFP and tdTomato proteins, when combined with the staining of nuclei obtained by the *in vivo* Hoechst labeling procedure, provided sufficient cellular and tissue morphology information to allow for the identification of intoxicated cells in unfixed and unprocessed organ slices. It should also be noted that although only excised organs were examined here, the assay should be adaptable for multiphoton intravital imaging of cellular intoxication with essentially no modifications needed.

In a broad survey of organs, intoxication was documented by confocal microscopy in the heart, lung, liver, kidney, spleen, esophagus, and bone marrow, whereas intoxication of the lymph nodes, thymus, intestine, uterus, trachea, tongue, skin, and brain was not observed. The latter tissues may not be exposed to sufficient toxin to allow for cellular entry and/or Cre-mediated recombination and/or may express no or insufficient CMG-2 and TEM-8. Alternatively, the confocal sections analyzed may not have captured the target cell population of a particular organ. In support of the latter, for five of the tissues in which intoxication was not observed by confocal microscopy, intoxication nevertheless could be detected by PCR.

The development of our novel imaging assay afforded the first opportunity to directly visualize CMG-2- and TEM-8-

mediated anthrax toxin intoxication and thereby enhance our understanding of the two receptors in the intoxication process. Intoxication was dependent on expression of either CMG-2 or TEM-8, as mice with combined deficiency in the two anthrax toxin receptors were refractory to intoxication in all organs analyzed. Previous genetic studies in mice have demonstrated that CMG-2 deficiency conferred far greater resistance to anthrax lethal toxin and *B. anthracis* spore exposure than TEM-8 deficiency and identified the heart and liver as key CMG-2-dependent targets for, respectively, anthrax lethal toxin and anthrax edema toxin (12, 52). Assuming that both receptors were close to ubiquitously expressed in tissues, this was tentatively suggested to be a consequence of a more than tenfold lower affinity of PA for TEM-8 than for CMG-2. These findings are compatible with the current imaging study, showing that TEM-8 was essentially unable to support the intoxication in the heart and liver, despite repeated toxin exposure through multiple injections. It should be noted, however, that full intoxication in other organs, including the spleen and kidney, was dependent upon TEM-8. This unequivocally demonstrates that TEM-8 is a functional receptor for anthrax toxin *in vivo* despite its reported lower affinity for PA and the reported primary importance of CMG-2 in whole-animal intoxication (12, 52).

A curious discrepancy between the aforementioned genetic studies and our current imaging study pertains to the intestine: Genetic studies have definitively established intestinal epithelial cells as direct targets for anthrax edema toxin (12). Nevertheless, we were consistently unable to observe the intoxication in intestinal epithelium. Intestinal epithelial cells of the $mTmG^{+/0}$ reporter mice have previously been shown to undergo recombination *in vivo* and express eGFP in response to constitutive or inducible Cre expression, showing that the *mTmG* transgene is not inherently refractory to Cre-mediated recombination in intestinal epithelium (51). An attractive explanation for this discrepancy pertains to the lack of toxicity of LFn-NLS-Cre/PA as compared with edema toxin. We speculate that edema toxin may initially be unable to access this barrier tissue, but because damage to other visceral organs progresses as a consequence of edema toxin intoxication, endothelial and/or epithelial barrier breakdown may allow entrance to the intestinal epithelial cells.

The imaging assay described here is simple and robust, and importantly, it does not require the handling of toxic proteins. Therefore, it should be amenable for and adaptable to diverse research settings. The assay should be useful for answering a number of basic research questions regarding the pathogenicity of anthrax toxins, as well as assisting clinical/translational efforts aimed at optimizing the treatment of individuals accidentally or deliberately exposed to *Bacillus anthracis*.

A potential limitation of the novel assay is that the Cre/LoxP system only allows for a binary readout as regards individual cells (nonintoxicated/intoxicated). In a whole-organ context, this should not prevent the generation of semiquantitative or quantitative data, as shown by the relationship between the toxin dose administered and the fluorescence intensity observed in individual organs. For such quantitative studies, the fraction of intoxicated cells in a given tissue could be enumerated by confocal image analysis. Alternatively, the ratio of green to red fluorescence could be determined in whole-organ extracts.

Considerable effort is currently being expended on the development of modified anthrax toxins as novel agents for the treatment of human malignancies. Strategies employed include the reengineering of PA to bind tumor cell surface-enriched proteins (33, 34), and the reengineering of PA to be proteolytically activated by proteases enriched in the tumor microenvironment, including matrix metalloproteinases (35–42), urokinase plasminogen activator (37, 39, 41, 44, 47, 53), and testisin (48). The assay described here is eminently suited for assessing the efficiency of LF delivery to tumor-relevant cell populations by these modified PAs, as well as to systematically delineate off-targets, which may be invaluable for dose and route of delivery optimization. Last, but not least, by using PA variants selectively cleaved by specific cell surface proteases (42, 45, 48), the assay may be used for *in vivo* imaging of specific cell surface proteolytic activity in diverse physiological and pathological settings.

## Experimental procedures

### Recombinant proteins

Plasmids for expressing proteins having LFn (LF aa 1–254) fused to Cre recombinase were constructed using the Champion pET SUMO vector (Invitrogen), which expresses proteins fused at the C-terminus of a His6-SUMO tag. DNA-encoding residues 1 to 254 of anthrax lethal factor originated from *Bacillus anthracis*, and those of Cre recombinase from bacteriophage P1. The sequences of the four LFn-Cre proteins are shown in Fig. S1. They differ only in the linker sequences. Two of the constructs contain ubiquitin between LFn and Cre, and three contain a nuclear localization signal (NLS) preceding Cre. The proteins were expressed as per the Champion pET SUMO manufacturer's instructions with minor modifications. Cell lysates were adsorbed to Ni-NTA resins, and the His-tagged proteins were eluted with imidazole solutions. The His6-SUMO-LFn-Cre proteins were cleaved with SUMO protease, which was made inhouse using Addgene plasmid #64697, deposited to Addgene by Dr Hideo Iwai (54). The His6-SUMO polypeptide and the His6-tagged SUMO protease were subtractively removed by passage through Ni-NTA resin. The LFn-Cre proteins were further purified by chromatography on hydroxyapatite to achieve purities of >95%. The LFn-NLS-Cre protein selected for the animal imaging studies was obtained in yields of >20 mg/l of culture.

### Cell culture assays

Efficacy of LFn-Cre protein translocation into cells was tested in CV1-5B cells (55, 56), which contain a single copy lox-stop-lox-β-galactosidase transgene. Cells were plated in 12- and 96-well plates in DMEM high-glucose medium with 10% fetal bovine serum, cultured at 37 °C at 10% $CO_2$, and used when they were at low and high confluency. PA and

LFn-Cre proteins were added at varying concentrations. After 40 h, the plates were washed in phosphate buffered saline (PBS) containing 2 mM $MgCl_2$ and fixed in PBS, 5 mM EGTA, 2 mM $MgCl_2$, and 0.2% glutaraldehyde for 30 min. After again washing in PBS with 2 mM $MgCl_2$, β-galactosidase activity was measured in two ways. For quantitative measurements, the 96-well plates were stained in PBS, 2 mM $MgCl_2$, 0.1% Triton X-100, 0.1% $NaN_3$, and 1 mg/ml chlorophenol red-β-D-galactopyranoside (CPRG) (57). Absorbance was measured at 570 nm after 20 min. In parallel, 12-well plates were stained with PBS, 2 mM $MgCl_2$, 5 mM potassium ferrocyanide, 5 mM potassium ferricyanide, 1 mg/ml 5-bromo-3-indolyl β-D-galactopyranoside (Bluo-Gal) for 5 h, and microscopy images were collected using a Nikon Eclipse TE2000-U microscope.

### Animal work

All experiments were performed in an Association for Assessment and Accreditation of Laboratory Animal Care International–accredited vivarium following Standard Operating Procedures and were approved by the NIAID Institutional Animal Care and Use Committee. B6.129(Cg)-*Gt(ROSA)26Sortm4(ACTB-tdTomato,-EGFP)Luo*/J$^{+/0}$ (*mTmG*$^{+/0}$ mice) were generated by crossing B6.129(Cg)-*Gt(ROSA)26Sortm4(ACTB-tdTomato,-EGFP)Luo*/J$^{+/+}$ (Jackson Laboratory) (51) males with C57BL/6J females (Jackson Laboratory). Wild-type C57BL/6J mice were used as controls. Both male and female mice were used for experiments at age 4 to 11 weeks. The generation of CMG-2- (*Cmg2*$^{-/-}$) and TEM-8- (*Tem8*$^{-/-}$) deficient mice has been described previously (52). *Cmg2*$^{-/-}$;*mTmG*$^{+/0}$, *Tem8*$^{-/-}$;*mTmG*$^{+/0}$ and *Cmg2*$^{-/-}$;*Tem8*$^{-/-}$;*mTmG*$^{+/0}$ mice were generated by interbreeding. The following primer pairs were used for genotyping: *Cmg2* wildtype allele, 5′-GACTCTTAGGAAGGGTTCCTACTGG-3′ and 5′-TGTAAGTCATATGGGTAGTGACCTAT-3′. *Cmg2* mutant allele, 5′-CCAATTTGGAGCTCAGGTTGGTGGA-3′ and 5′-TGTAAGTCATATGGGTAGTGACCTAT-3′. *Tem8* wildtype allele, 5′-ATGTCCCTTTGCCTCTTGTGGC-3′ and 5′- TTCCACCTCACTGACCACCC-3′. *Tem8* mutant allele, 5′-AGGCACTGACAAACCCTCTCAGGA-3′ and 5′-CCAGCCCATGCTGACAGCTCACAGA-3′.

### PCR analysis of Cre-mediated recombination in mouse organs

The protein mixture containing 25 μg of LFn-NLS-Cre and 25 μg of PA in PBS was delivered *via* tail vein injection into *mTmG*$^{+/0}$ mice. After 24 h, the mice were euthanized by $CO_2$ inhalation. Organs and bone marrow were digested overnight in lysis buffer (100 mM Tris HCl, pH 8, 5 mM EDTA, 200 mM NaCl, 0.2% SDS, and 100 mg/ml Proteinase K) at 55 °C. DNA was precipitated using isopropanol. PCR was performed with the following primers: GFP RV: 5′-CGTCGCCGTCCAGCTCGACCAG-3′, Tomato RV: 5′-GCCCATGAACTCTTTGATGACCTCCTCTCCC-3′, and LoxP FW: 5′-CCGCGGGCTCGACACTGAACC-3′ using JumpStart REDTaq ReadyMix (Sigma). PCR products were separated on 1.5% agarose gels, stained with ethidium bromide, and visualized by UV illumination. Cre recombination resulted in a PCR product (LoxP FW + GFP RV) of 258 bp, while the nonrecombinant PCR product (LoxP FW + Tomato RV) was 157 bp.

### Imaging anthrax toxin intoxication in mice

LFn-NLS-Cre and PA proteins alone or in combination in PBS were delivered intraperitoneally or *via* tail vein injection. The mice were tail vein-injected with 100 μl of 6 mg/ml Hoechst 33342 dye (Thermo Fisher Scientific) 4 to 6 h prior to termination of an experiment to visualize nuclei (58). Mice were euthanized by $CO_2$ inhalation and perfused with ice-cold PBS using cardiac puncture. Organs were immediately removed and cut into ∼1 to 2 mm thick slices using a scalpel. The organ slices were placed on a MatTek glass bottom microwell dish (MatTek Corporation) and imaged using a 20× 0.75 NA Air or 60× 1.27 NA Water objective (Nikon) on an A1R + MP confocal microscope system (Nikon). Large images were composed of stitched images with a 10% overlap using NIS-Elements software (Nikon).

### Flow cytometry

Single-cell suspensions from spleens were stained with the Live/Dead Cell Viability assay (Invitrogen), and cell surface markers were stained with the following anti-mouse antibodies at 1:200 dilution per $10^6$ cells: Ly6C (AL-21; BD Biosciences), Ly6G (1A8; BD Biosciences), B220 (RA3-6B2; BioLegend), CD11B (M1/70; BioLegend), TCRb (H57-597; BioLegend), CD11C (N418; BioLegend), and CD45 (30.F11; eBioscience). All samples were analyzed using a FACS Fortessa cytometer (BD Biosciences).

## Data availability

All data presented and discussed in the article are contained within the body of article and supporting figures.

*Supporting information*—This article contains supporting information.

*Acknowledgments*—We thank Annika Schmidt, Carolyn Robb, Pia Mittweg, and Yongguang Jiang for technical assistance. We thank Dr Mary Jo Danton for critically reviewing this manuscript.

*Author contributions*—C. M., E. M. C., L. M. S., M. M., D. P., S. N., R. H., S. H. L., and T. H. B. conceptualization; C. M., E. M. C., S. H. L., and T. H. B. data curation; C. M., E. M. C., R. J. F., L. M. S., M. M., S. H. L., and T. H. B. formal analysis; S. H. L. and T. H. B. funding acquisition; C. M., E. M. C., R. J. F., L. M. S., Q. Q. M., M. M., D. P., S. N., R. H., S. H. L., and T. H. B. investigation; C. M., E. M. C., L. M. S., S. H. L., and T. H. B. methodology; C. M., E. M. C., Q. Q. M., M. M., and T. H. B. project administration; R. J. F., Q. Q. M., M. M., S. H. L., and T. H. B. resources; M. M., S. H. L., and T. H. B. supervision; C. M., E. M. C., and L. M. S. validation; C. M., E. M. C., and L. M. S. visualization; C. M., E. M. C., L. M. S., S. H. L., and T. H. B. writing—original draft; C. M., E. M. C., R. J. F., L. M. S., M. M., D. P., S. N., R. H., S. H. L., and T. H. B. writing—review and editing.

*Funding and additional information*—Supported by the NIAID (S. H. L.) and NIDCR Intramural Research Program (T. H. B.) of the

NIH, NIDCR 1K99DE030124-01A1 (L. M. S.), and the NIDCR Combined Technical Research Core (ZIC DE000729-09) and NIDCR Imaging Core: ZIC DE000750-01. R. H., S. N., and D. P. were funded by the European Union's Horizon 2020 research and innovation program grant agreement No. 686841 (MAGNEURON). The content is solely the responsibility of the authors and does not necessarily represent the official views of the National Institutes of Health.

*Conflict of interest*—The authors declare no competing financial interests in relation to the work described.

*Abbreviations*—The abbreviations used are: CMG-2, capillary morphogenesis protein-2; EF, edema factor; LF, lethal factor; LFn-NLS-Cre, LF fused to a nuclear localization signal-tagged Cre recombinase; NLRP1, NLR family pyrin domain containing 1; PA, protective antigen; TEM-8, tumor endothelial marker-8.

## References


1. Leppla, S. H., Robbins, J. B., Schneerson, R., and Shiloach, J. (2002) Development of an improved vaccine for anthrax. *J. Clin. Invest.* **110**, 141–144
2. Collier, R. J., and Young, J. A. (2003) Anthrax toxin. *Annu. Rev. Cell Dev. Biol.* **19**, 45–70
3. Bradley, K. A., Mogridge, J., Mourez, M., Collier, R. J., and Young, J. A. (2001) Identification of the cellular receptor for anthrax toxin. *Nature* **414**, 225–229
4. Scobie, H. M., Rainey, G. J., Bradley, K. A., and Young, J. A. (2003) Human capillary morphogenesis protein 2 functions as an anthrax toxin receptor. *Proc. Natl. Acad. Sci. U. S. A.* **100**, 5170–5174
5. Gordon, V. M., Klimpel, K. R., Arora, N., Henderson, M. A., and Leppla, S. H. (1995) Proteolytic activation of bacterial toxins by eukaryotic cells is performed by furin and by additional cellular proteases. *Infect. Immun.* **63**, 82–87
6. Mogridge, J., Cunningham, K., and Collier, R. J. (2002) Stoichiometry of anthrax toxin complexes. *Biochemistry* **41**, 1079–1082
7. Mogridge, J., Cunningham, K., Lacy, D. B., Mourez, M., and Collier, R. J. (2002) The lethal and edema factors of anthrax toxin bind only to oligomeric forms of the protective antigen. *Proc. Natl. Acad. Sci. U. S. A.* **99**, 7045–7048
8. Leppla, S. H. (1982) Anthrax toxin edema factor: A bacterial adenylate cyclase that increases cyclic AMP concentrations of eukaryotic cells. *Proc. Natl. Acad. Sci. U. S. A.* **79**, 3162–3166
9. Duesbery, N. S., Webb, C. P., Leppla, S. H., Gordon, V. M., Klimpel, K. R., Copeland, T. D., Ahn, N. G., Oskarsson, M. K., Fukasawa, K., Paull, K. D., and Vande Woude, G. F. (1998) Proteolytic inactivation of MAP-kinase-kinase by anthrax lethal factor. *Science* **280**, 734–737
10. Mendenhall, M. A., Liu, S., Portley, M. K., O'Mard, D., Fattah, R., Szabo, R., Bugge, T. H., Khillan, J. S., Leppla, S. H., and Moayeri, M. (2020) Anthrax lethal factor cleaves regulatory subunits of phosphoinositide-3 kinase to contribute to toxin lethality. *Nat. Microbiol.* **5**, 1464–1471
11. Levinsohn, J. L., Newman, Z. L., Hellmich, K. A., Fattah, R., Getz, M. A., Liu, S., Sastalla, I., Leppla, S. H., and Moayeri, M. (2012) Anthrax lethal factor cleavage of Nlrp1 is required for activation of the inflammasome. *PLoS Pathog.* **8**, e1002638
12. Liu, S., Zhang, Y., Moayeri, M., Liu, J., Crown, D., Fattah, R. J., Wein, A. N., Yu, Z. X., Finkel, T., and Leppla, S. H. (2013) Key tissue targets responsible for anthrax-toxin-induced lethality. *Nature* **501**, 63–68
13. Moayeri, M., Leppla, S. H., Vrentas, C., Pomerantsev, A. P., and Liu, S. (2015) Anthrax pathogenesis. *Annu. Rev. Microbiol.* **69**, 185–208
14. Arora, N., and Leppla, S. H. (1993) Residues 1-254 of anthrax toxin lethal factor are sufficient to cause cellular uptake of fused polypeptides. *J. Biol. Chem.* **268**, 3334–3341
15. Leppla, S. H., Arora, N., and Varughese, M. (1999) Anthrax toxin fusion proteins for intracellular delivery of macromolecules. *J. Appl. Microbiol.* **87**, 284
16. Arora, N., and Leppla, S. H. (1994) Fusions of anthrax toxin lethal factor with shiga toxin and diphtheria toxin enzymatic domains are toxic to mammalian cells. *Infect. Immun.* **62**, 4955–4961
17. Arora, N., Klimpel, K. R., Singh, Y., and Leppla, S. H. (1992) Fusions of anthrax toxin lethal factor to the ADP-ribosylation domain of Pseudomonas exotoxin A are potent cytotoxins which are translocated to the cytosol of mammalian cells. *J. Biol. Chem.* **267**, 15542–15548
18. Sharma, M., Khanna, H., Arora, N., and Singh, Y. (2000) Anthrax toxin-mediated delivery of cholera toxin-a subunit into the cytosol of mammalian cells. *Biotechnol. Appl. Biochem.* **32**, 69–72
19. Hobson, J. P., Liu, S., Rono, B., Leppla, S. H., and Bugge, T. H. (2006) Imaging specific cell-surface proteolytic activity in single living cells. *Nat. Methods* **3**, 259–261
20. Mehra, V., Khanna, H., Chandra, R., and Singh, Y. (2001) Anthrax-toxin-mediated delivery of a 19 kDa antigen of Mycobacterium tuberculosis into the cytosol of mammalian cells. *Biotechnol. Appl. Biochem.* **33**, 71–74
21. Zornetta, I., Brandi, L., Janowiak, B., Dal Molin, F., Tonello, F., Collier, R. J., and Montecucco, C. (2010) Imaging the cell entry of the anthrax oedema and lethal toxins with fluorescent protein chimeras. *Cell. Microbiol.* **12**, 1435–1445
22. Goletz, T. J., Klimpel, K. R., Arora, N., Leppla, S. H., Keith, J. M., and Berzofsky, J. A. (1997) Targeting HIV proteins to the major histocompatibility complex class I processing pathway with a novel gp120-anthrax toxin fusion protein. *Proc. Natl. Acad. Sci. U. S. A.* **94**, 12059–12064
23. Moriya, O., Matsui, M., Osorio, M., Miyazawa, H., Rice, C. M., Feinstone, S. M., Leppla, S. H., Keith, J. M., and Akatsuka, T. (2001) Induction of hepatitis C virus-specific cytotoxic T lymphocytes in mice by immunization with dendritic cells treated with an anthrax toxin fusion protein. *Vaccine* **20**, 789–796
24. Zhang, Y., Kida, Y., Kuwano, K., Misumi, Y., Ikehara, Y., and Arai, S. (2001) Role of furin in delivery of a CTL epitope of an anthrax toxin-fusion protein. *Microbiol. Immunol.* **45**, 119–125
25. Doling, A. M., Ballard, J. D., Shen, H., Krishna, K. M., Ahmed, R., Collier, R. J., and Starnbach, M. N. (1999) Cytotoxic T-lymphocyte epitopes fused to anthrax toxin induce protective antiviral immunity. *Infect. Immun.* **67**, 3290–3296
26. Liu, X. H., Collier, R. J., and Youle, R. J. (2001) Inhibition of axotomy-induced neuronal apoptosis by extracellular delivery of a Bcl-XL fusion protein. *J. Biol. Chem.* **276**, 46326–46332
27. Ballard, J. D., Doling, A. M., Beauregard, K., Collier, R. J., and Starnbach, M. N. (1998) Anthrax toxin-mediated delivery *in vivo* and *in vitro* of a cytotoxic T- lymphocyte epitope from ovalbumin. *Infect. Immun.* **66**, 615–619
28. Wesche, J., Elliott, J. L., Falnes, P. O., Olsnes, S., and Collier, R. J. (1998) Characterization of membrane translocation by anthrax protective antigen. *Biochemistry* **37**, 15737–15746
29. Paliga, D., Raudzus, F., Leppla, S. H., Heumann, R., and Neumann, S. (2019) Lethal factor domain-mediated delivery of Nurr1 transcription factor enhances tyrosine hydroxylase activity and protects from neurotoxin-induced degeneration of dopaminergic cells. *Mol. Neurobiol.* **56**, 3393–3403
30. Singh, Y., Klimpel, K. R., Goel, S., Swain, P. K., and Leppla, S. H. (1999) Oligomerization of anthrax toxin protective antigen and binding of lethal factor during endocytic uptake into mammalian cells. *Infect. Immun.* **67**, 1853–1859
31. Xavier, M. E., Liu, S., Bugge, T. H., Baguna-Torres, J., Mosley, M., Hopkins, S. L., Allen, P. D., Berridge, G., Vendrell, I., Fisher, R., Kersemans, V., Smart, S., Leppla, S. H., and Cornelissen, B. (2019) Tumor imaging using radiolabelled matrix metalloproteinase-activated anthrax proteins. *J. Nucl. Med.* **60**, 1474–1482
32. Briones, G., Hofreuter, D., and Galan, J. E. (2006) Cre reporter system to monitor the translocation of type III secreted proteins into host cells. *Infect. Immun.* **74**, 1084–1090

33. McCluskey, A. J., and Collier, R. J. (2013) Receptor-directed chimeric toxins created by sortase-mediated protein fusion. *Mol. Cancer Ther.* **12**, 2273–2281
34. McCluskey, A. J., Olive, A. J., Starnbach, M. N., and Collier, R. J. (2013) Targeting HER2-positive cancer cells with receptor-redirected anthrax protective antigen. *Mol. Oncol.* **7**, 440–451
35. Alfano, R. W., Leppla, S. H., Liu, S., Bugge, T. H., Meininger, C. J., Lairmore, T. C., Mulne, A. F., Davis, S. H., Duesbery, N. S., and Frankel, A. E. (2009) Matrix metalloproteinase-activated anthrax lethal toxin inhibits endothelial invasion and neovasculature formation during *in vitro* morphogenesis. *Mol. Cancer Res.* **7**, 452–461
36. Alfano, R. W., Leppla, S. H., Liu, S., Bugge, T. H., Ortiz, J. M., Lairmore, T. C., Duesbery, N. S., Mitchell, I. C., Nwariaku, F., and Frankel, A. E. (2010) Inhibition of tumor angiogenesis by the matrix metalloproteinase-activated anthrax lethal toxin in an orthotopic model of anaplastic thyroid carcinoma. *Mol. Cancer Ther.* **9**, 190–201
37. Liu, S., Redeye, V., Kuremsky, J. G., Kuhnen, M., Molinolo, A., Bugge, T. H., and Leppla, S. H. (2005) Intermolecular complementation achieves high-specificity tumor targeting by anthrax toxin. *Nat. Biotechnol.* **23**, 725–730
38. Liu, S., Wang, H., Currie, B. M., Molinolo, A., Leung, H. J., Moayeri, M., Basile, J. R., Alfano, R. W., Gutkind, J. S., Frankel, A. E., Bugge, T. H., and Leppla, S. H. (2008) Matrix metalloproteinase-activated anthrax lethal toxin demonstrates high potency in targeting tumor vasculature. *J. Biol. Chem.* **283**, 529–540
39. Peters, D. E., Hoover, B., Grey Cloud, L., Liu, S., Molinolo, A. A., Leppla, S. H., and Bugge, T. H. (2014) Comparative toxicity and efficacy of engineered anthrax lethal toxin variants with broad anti-tumor activities. *Toxicol. Appl. Pharmacol.* **279**, 220–229
40. Phillips, D. D., Fattah, R. J., Crown, D., Zhang, Y., Liu, S., Moayeri, M., Fischer, E. R., Hansen, B. T., Ghirlando, R., Nestorovich, E. M., Wein, A. N., Simons, L., Leppla, S. H., and Leysath, C. E. (2013) Engineering anthrax toxin variants that exclusively form octamers and their application to targeting tumors. *J. Biol. Chem.* **288**, 9058–9065
41. Schafer, J. M., Peters, D. E., Morley, T., Liu, S., Molinolo, A. A., Leppla, S. H., and Bugge, T. H. (2011) Efficient targeting of head and neck squamous cell carcinoma by systemic administration of a dual uPA and MMP-activated engineered anthrax toxin. *PLoS One* **6**, e20532
42. Liu, S., Netzel-Arnett, S., Birkedal-Hansen, H., and Leppla, S. H. (2000) Tumor cell-selective cytotoxicity of matrix metalloproteinase-activated anthrax toxin. *Cancer Res.* **60**, 6061–6067
43. Abi-Habib, R. J., Singh, R., Leppla, S. H., Greene, J. J., Ding, Y., Berghuis, B., Duesbery, N. S., and Frankel, A. E. (2006) Systemic anthrax lethal toxin therapy produces regressions of subcutaneous human melanoma tumors in athymic nude mice. *Clin. Cancer Res.* **12**, 7437–7443
44. Liu, S., Aaronson, H., Mitola, D. J., Leppla, S. H., and Bugge, T. H. (2003) Potent antitumor activity of a urokinase-activated engineered anthrax toxin. *Proc. Natl. Acad. Sci. U. S. A.* **100**, 657–662
45. Liu, S., Bugge, T. H., and Leppla, S. H. (2001) Targeting of tumor cells by cell surface urokinase plasminogen activator-dependent anthrax toxin. *J. Biol. Chem.* **276**, 17976–17984
46. Rono, B., Romer, J., Liu, S., Bugge, T. H., Leppla, S. H., and Kristjansen, P. E. (2006) Antitumor efficacy of a urokinase activation-dependent anthrax toxin. *Mol. Cancer Ther.* **5**, 89–96
47. Su, Y., Ortiz, J., Liu, S., Bugge, T. H., Singh, R., Leppla, S. H., and Frankel, A. E. (2007) Systematic urokinase-activated anthrax toxin therapy produces regressions of subcutaneous human non-small cell lung tumor in athymic nude mice. *Cancer Res.* **67**, 3329–3336
48. Martin, E. W., Buzza, M. S., Driesbaugh, K. H., Liu, S., Fortenberry, Y. M., Leppla, S. H., and Antalis, T. M. (2015) Targeting the membrane-anchored serine protease testisin with a novel engineered anthrax toxin prodrug to kill tumor cells and reduce tumor burden. *Oncotarget* **6**, 33534–33553
49. Bachran, C., Morley, T., Abdelazim, S., Fattah, R. J., Liu, S., and Leppla, S. H. (2013) Anthrax toxin-mediated delivery of the Pseudomonas exotoxin A enzymatic domain to the cytosol of tumor cells via cleavable ubiquitin fusions. *mBio* **4**, e00201–e00213
50. Le, Y., Gagneten, S., Tombaccini, D., Bethke, B., and Sauer, B. (1999) Nuclear targeting determinants of the phage P1 cre DNA recombinase. *Nucleic Acids Res.* **27**, 4703–4709
51. Muzumdar, M. D., Tasic, B., Miyamichi, K., Li, L., and Luo, L. (2007) A global double-fluorescent Cre reporter mouse. *Genesis* **45**, 593–605
52. Liu, S., Crown, D., Miller-Randolph, S., Moayeri, M., Wang, H., Hu, H., Morley, T., and Leppla, S. H. (2009) Capillary morphogenesis protein-2 is the major receptor mediating lethality of anthrax toxin *in vivo*. *Proc. Natl. Acad. Sci. U. S. A.* **106**, 12424–12429
53. Abi-Habib, R. J., Singh, R., Liu, S., Bugge, T. H., Leppla, S. H., and Frankel, A. E. (2006) A urokinase-activated recombinant anthrax toxin is selectively cytotoxic to many human tumor cell types. *Mol. Cancer Ther.* **5**, 2556–2562
54. Guerrero, F., Ciragan, A., and Iwai, H. (2015) Tandem SUMO fusion vectors for improving soluble protein expression and purification. *Protein Expr. Purif.* **116**, 42–49
55. Peitz, M., Jager, R., Patsch, C., Jager, A., Egert, A., Schorle, H., and Edenhofer, F. (2007) Enhanced purification of cell-permeant Cre and germline transmission after transduction into mouse embryonic stem cells. *Genesis* **45**, 508–517
56. Kellendonk, C., Tronche, F., Monaghan, A. P., Angrand, P. O., Stewart, F., and Schutz, G. (1996) Regulation of Cre recombinase activity by the synthetic steroid RU 486. *Nucleic Acids Res.* **24**, 1404–1411
57. Sicard, C., Shek, N., White, D., Bowers, R. J., Brown, R. S., and Brennan, J. D. (2014) A rapid and sensitive fluorimetric beta-galactosidase assay for coliform detection using chlorophenol red-beta-D-galactopyranoside. *Anal. Bioanal. Chem.* **406**, 5395–5403
58. Madsen, D. H., Jurgensen, H. J., Siersbaek, M. S., Kuczek, D. E., Grey Cloud, L., Liu, S., Behrendt, N., Grontved, L., Weigert, R., and Bugge, T. H. (2017) Tumor-associated macrophages derived from circulating inflammatory monocytes degrade collagen through cellular uptake. *Cell Rep.* **21**, 3662–3671